Novel Fast Multiline Analysis of Parasitic Effects in CPW Inductors for MMIC's

I. Huynen, *Member, IEEE*

***Abstract*— This letter presents a novel multiline modeling of monolithic microwave integrated circuit (MMIC) spiral inductors in coplanar waveguide (CPW) technology. Starting from transmission line parameters calculated for only single lines and pairs of lines, a distributed equivalent circuit is established for each section of multicoupled lines in the structure. It readily yields the S-parameters of the section. An adequate interconnection of sections having different topologies results in the S-matrix of the device. Our technique is wideband, fast, and fully scalable. It predicts on-line the effect of the underpass and of spurious propagation along the coplanar waveguide (CPW) grounding. It is shown that a significant frequency shift is due to the combination of those two effects. Results are validated by measurements on SOI inductors, up to the second self-resonance frequency.**

I. Introduction

With the growing demand for radio frequency (RF) and mobile communications, many efforts concentrate on establishing design rules for wideband monolithic microwave integrated circuit (MMIC) spiral inductors. Electromagnetic simulators (EMS's) offer a wideband analysis of spiral devices, based on a full-wave modeling of multicoupled lines [1]. However, the computation time increases with the number of turns of the spiral and the ratio line width to line spacing [2]. It rapidly becomes too large for on-line design and optimization tasks. Many EMS's are also unable to take into account the frequency dependence of the bulk resistivity [1]. Hence, monolithic microwave integrated circuit (MMIC) designers prefer to build a lumped-element π-equivalent circuit for the spiral inductor. The value of the elements is obtained by fitting the S-parameters of the π-circuit to measured data [3]. Users argue that fitting is much faster than other numerical tools [2], and that the π-circuit is easily inserted in a circuit simulator. The model, however, is not scalable. Fitted elements are frequency- and technology-dependent [4], and the fitting accuracy deteriorates when bulk resistivity decreases [3]. More importantly, the lumped-element model is not valid above the first self-resonance frequency [2].

In this letter, an efficient multiline analysis of spiral inductors is presented. It is based on a judicious combination of transmission line parameters (TLP's) computed for only single lines and pairs of lines of various topologies. TLP form a distributed system which is readily solved by an explicit coupled line theory. Using this new approach, the behavior of the device is described over a wide band, with a very reduced numerical complexity. TLP's of single lines and pairs of lines can be rapidly obtained by using efficient analytical expressions [5], [6], and the computation time is reduced. Those expressions are function of the geometrical and electrical parameters of the various layers, (semi)conductive or not. Hence, the scalability of our model is ensured. The model predicts a shift of the self-resonance frequencies induced by the underpassing contact, due to parasitic propagation along the CPW groundings. Results are experimentally validated up to the second self-resonance frequency.

Manuscript received September 19, 1997. This work was supported by the National Fund for Scientific Research, Belgium, by the "Communauté Francaise de Belgique," through the Program "Actions de Recherche Concertées," Belgium, and by the ESPRIT Project 24 006 of the European Communities.

The author is with Microwaves U.C.L., Batiment Maxwell, B-1348 Louvain-la-Neuve, Belgium.

Publisher Item Identifier S 1051-8207(98)01461-5.

II. Description of the Model

The device consists of aluminum strips buried in a SiO_2 layer lying on a resistive silicon wafer having a metallic plane on its backside. Fig. 1(a) shows the spiral in the plane of the first metal level (M1). It is surrounded by a metallic pad to ensure adequate grounding for the coplanar waveguide (CPW) accesses. The center of the spiral is connected to the CPW access by an underpassing metal strip (level M2) buried in a SiO_2 layer between the plane M1 and the Si layer on the backside. Another SiO_2 layer exists above the M1 level.

The spiral is first divided into several sets of n-coupled microstrip lossy lines. We build the distributed circuit of a n-strip section from that corresponding to a single pair of lossy strips. Each strip is described by single (L, C) elements and influenced only by its two adjacent strips via mutual capacitances C_m and inductances L_m. The values of the elements are taken equal to those of the distributed equivalent circuit of a pair of coupled symmetric lines [7], as a function of their even and odd TLP:

$$L = \frac{\gamma_e Z_e + \gamma_o Z_o}{2j\omega}, \quad L_m = \frac{\gamma_e Z_e - \gamma_o Z_o}{2j\omega} \tag{1a}$$

$$C = \frac{\gamma_e}{j\omega Z_e}, \quad C_m = \frac{\gamma_o}{2j\omega Z_o} - \frac{\gamma_e}{2j\omega Z_e} \tag{1b}$$

where $\gamma_{e,o}$ is the complex propagation constant of, respectively, the even and odd mode supported by the pair of lines, and $Z_{e,o}$ their respective complex characteristic impedance. We obtain those TLP from a variational formalism [5], taking into account the geometrical and technological parameters. The two SiO_2 layers and the Si layer are considered when calculating the TLP of line sections in Fig. 1(a), except for the slot and 5-coupled strip sections above the underpass. The M2 strip acts as a ground plane, hence the Si layer is neglected for those sections.

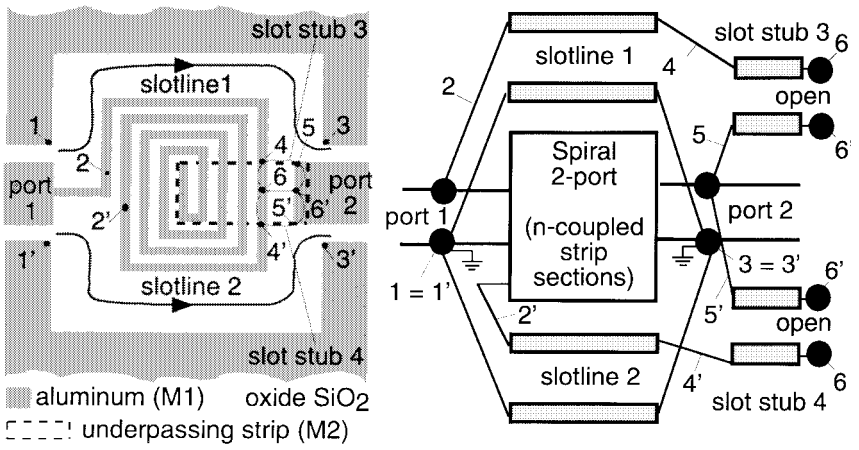

(a) (b)

Fig. 1. CPW spiral inductor in SOI technology (strips 16-μm width, 16-μm spacing, between two SiO_2 layers 1 μm thick lying on Si wafer 500 μm thick, Si resistivity 100 Ω/cm, aluminum metal, mean distance from spiral to metallic pads 65 μm). (a) Layout in plane of first metallization level (M1). (b) Modeling of propagation paths along CPW groundings.

A conventional system of $2n$ first-order differential equations relates the voltage and current on the n lines of the section. Assuming that voltages and currents have the same $e^{-\gamma z}$ dependency on each of the n lines, the system reduces to two second-order systems:

$$-\gamma^2 \overline{V} = -\omega^2 \overline{\overline{L}} \cdot \overline{\overline{C}}\, \overline{V} \tag{2a}$$

$$-\gamma^2 \overline{I} = -\omega^2 \overline{\overline{L}} \cdot \overline{\overline{C}}\, \overline{I} \tag{2b}$$

where $\overline{V}$ and $\overline{I}$ are column-vectors of size n, describing the voltages and currents on each of the n lines, and $\overline{\overline{L}}, \overline{\overline{C}}$ are inductance and capacitance matrices whose coefficients are linear combinations of the elements. The general solution of system (2) is a linear combination of its $2n$ eigensolutions

$$\overline{V(z)} = \sum_{k=1}^{n} (A_k e^{-\gamma_k z} + B_k e^{\gamma_k z}) \overline{V}_k \tag{3a}$$

$$\overline{I(z)} = \sum_{k=1}^{n} (A_k e^{-\gamma_k z} - B_k e^{\gamma_k z}) \overline{I}_k \tag{3b}$$

where γ_k is the kth eigenvalue of system (2) and $\overline{V}_k, \overline{I}_k$, are the associated vectors of voltages and currents on the n lines. Using (2) and (3), the *implicit* eigenvalue problem associated to full-wave methods is replaced by a simple *explicit* eigenvalue problem, which is a main advantage. Values of (3) taken at $z = 0$ and $z = L$ are currents and voltages at the $2n$ accesses of the equivalent $2n$-port. Feeding one access (port i) and loading the others by a reference impedance Z_r yields $2n$ equations to be solved for the set of coefficients $\{A_k, B_k\}$. After transforming S- into Y-parameters, the n-strip sections forming the spiral are interconnected.

Additional RF paths are generated by the slotlines 1, 2 between the spiral and the groundings and by the open-ended slotlines 3, 4 existing between the spiral and port 2 (Fig. 1). Slotline TLP's are computed depending on the number of layers (SiO_2/M1/SiO_2/Si/ground for slotlines 1 and 2, and SiO_2/M1/SiO_2/M2 for slot stubs 3 and 4). The Y-matrices of slotlines 1, 2 are connected as shown in Fig. 1(b), from nodes 2, 1 to 4, 3 for slot 1, and from nodes 2′, 1′ to 4′, 3′ for slot 2. (Node 2′ is internal to the spiral 2-port model.) The capacitance and inductance created by the metallic pads are thus modelled in a distributed manner, since a transmission line is a cascade of infinitesimal (L, C) cells. Similarly, slot stubs 3 and 4 are used from nodes 6, 6′ to nodes 4, 5 and 4′, 5′, respectively. They model the coupling between the outer turn of the spiral and the center conductor of CPW port 2. Nodes 3, 3′, 1, 1′ are connected to the ground plane of the spiral strips, as done for measurement.

III. Experimental Validation of the Model

The relevance of our approach is illustrated in Fig. 2. Fig. 2(a) compares the transmission parameter S_{12} of the spiral inductor in Fig. 1 calculated using our model under various assumptions. Curve 1 is obtained assuming no coupling between the turns of the spiral ($C_m = L_m = 0$ for each multicoupled section) and no underpassing strip (TLP computed with SiO_2/M1/SiO_2/Si/ground for all line sections). A poor agreement is observed: the device is in fact modeled as a single lossy 100-Ω line. Curve 2 takes coupling into account: the reactive elements C_m and L_m limits the transmission level at high frequencies. Curve 3 takes into account both coupling and underpassing strip, where only the two SiO_2 layers are considered when computing TLP in the underpass area. The transmission parameter S_{12} exhibits resonance peaks: the modification of TLP in the underpass area limits the self-resonance frequency of the spiral. Our final modeling (curve 4) takes into account the influence of the additional paths for the RF signal, modeled by slotlines as depicted in Fig. 1(b), and a shift of the first and second resonant peaks occurs. As shown in Fig. 2(b), S-parameters simulated using the complete model of Fig. 1(b) and (1)–(3) exhibit a very good agreement with measurements (dashed curve). A similar agreeement is obtained for the reflection coefficients and for the phases (not shown here). As expected, the lumped RLCG elements of an equivalent π-network extracted from the modeled S-parameters correspond to those extracted from measured ones. The agreement is illustrated in Fig. 3(a) for the R and L lumped elements associated to the series branch of the network: this branch

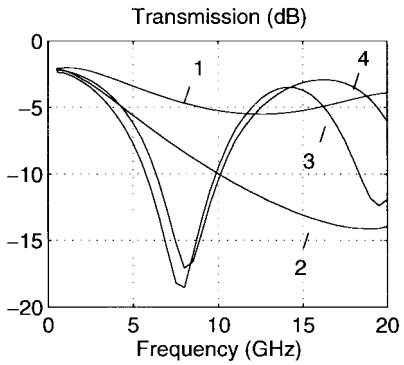

(a)

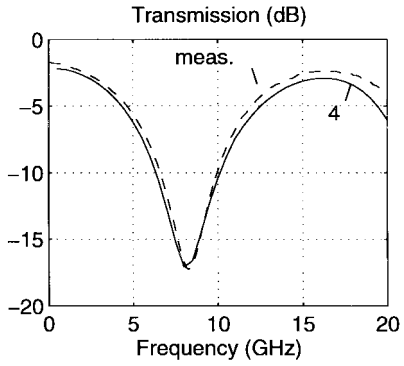

(b)

Fig. 2. Magnitude of transmission factor S_{12} (a) 1: without coupling, underpassing, and CPW grounding effects; 2: with coupling only; 3: with coupling and underpassing effect; 4: with coupling, underpassing, and CPW grounding effects according to Fig. 1(b). (b) Comparison of 4 (solid) with measurements (dashed).

becomes capacitive between 8 and 16 GHz. Our model is thus valid above the first self-resonance: this is because it uses adequate connections of transmission lines which are able to model the slotline paths and the multiconductor topology specific to each device over a wider band than lumped elements. The same agreement is obtained for the shunt elements (not shown), hence for the Q factor [Fig. 3(b)]. Our modeling is carried out on a Sun Sparc Ultra 2, using Matlab 4.2 software, in less than 0.5 s per frequency point. This has to be compared to the data given by authors in [2]: on a similar computer, a three-dimensional (3-D) simulator needs 5 min/frequency, while the extraction of their own lumped-elements π-network requires 2 min/frequency.

IV. Conclusion

We have developed a simplified multiline approach which efficiently predicts parasitic phenomena in the spiral inductor with CPW accesses. Calculations are fast, due to a judicious combination of TLP computation with coupled line theory, and results agree with experiment up to the second self-resonance. Using this multiline model 2-turns spiral and meander inductors have been modeled with a similar efficiency, as shown in [8].

References

[1] D. Lovelace, N. Camilleri, and G. Kannell, "Silicon MMIC inductor modeling for high volume, low cost applications," *Microwave J.*, pp. 60–71, Aug. 1994.

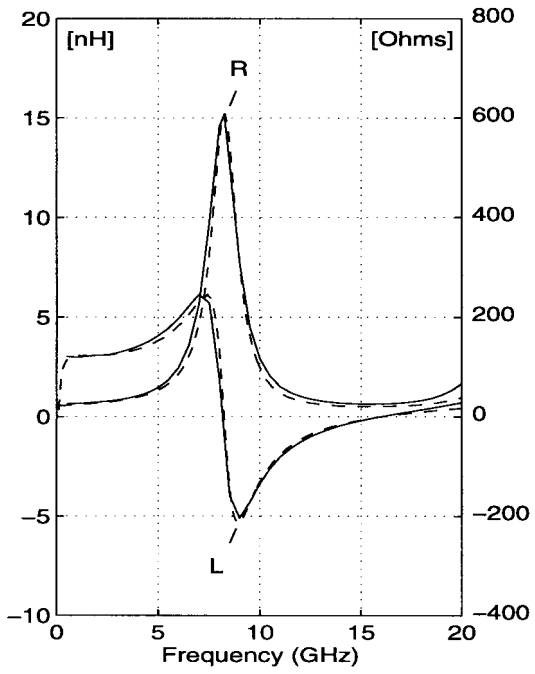

(a)

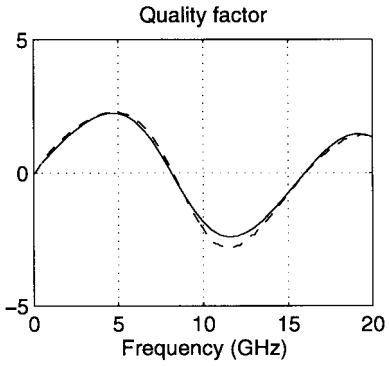

(b)

Fig. 3. Comparison between values for equivalent lumped-element π-network extracted from S-parameters modeled (solid) and measured (dashed). (a) Equivalent resistance R and inductance L of inductive branch in π-network. (b) Quality factor.

[2] J. R. Long and M. A. Copeland, "The modeling, characterization, and design of monolithic inductors for silicon RF IC's," *IEEE J. Solid-State Circuits*, vol. 32, pp. 357–368, Mar. 1997.
[3] M. Park, S. Lee, H. K. Yu, and J. G. Koo, "High Q CMOS-compatible microwave inductors using double-metal interconnection silicon technology," *IEEE Microwave Guided Wave Lett.*, vol. 7, pp. 45–47, Feb. 1997.
[4] C. P. Yue, C. Ryu, J. Lau, T. H. Lee, and S. S. Wong, "A physical model for planar spiral inductors on silicon," in *Proc. Int. Electron. Dev. Meeting*, vol. IEDM-95, pp. 6.5.1–6.5.4.
[5] I. Huynen, D. Vanhoenacker-Janvier, and A. Vander Vorst, "Spectral domain form of new variational expression for very fast calculation of multilayered lossy planar line parameters," *IEEE Trans. Microwave Theory Tech.*, vol. 42, pp. 2099–2106, Nov. 1994.
[6] M. Kirshning and R. H. Jansen, "Accurate wide range design equations for the frequency-dependent characteristics of parallel coupled microstrip lines," *IEEE Trans. Microwave Theory Tech.*, vol. MTT-32, pp. 83–90, Jan. 1984.
[7] R. K. Hoffmann, *Handbook of Microwave Integrated Circuits.* London, U.K.: Artech House, 1987.
[8] I. Huynen, J.-P. Raskin, R. Gillon, D. Vanhoenacker, and J.-P. Colinge, "Integrated microwave inductors on silicon-on-insulator substrate," in *Proc. 27th Eur. Microwave Conf.*, Jerusalem, Sept. 5–8, 1997, pp. 1008–1013.